Capturing Oscillator Injection Locking via Nonlinear Phase-Domain Macromodels

Xiaolue Lai and Jaijeet Roychowdhury

Abstract—Injection locking is a nonlinear dynamical phenomenon that is often exploited in electronic and optical oscillator design. Behavioral modeling techniques for oscillators that predict this phenomenon accurately are of significant scientific and practical importance. In this paper, we propose a nonlinear approach for generating small phase-domain oscillator/voltage-controlled oscillator (VCO) macromodels that capture injection locking well. Our nonlinear phase-domain macromodels are closely related to recent oscillator phase noise and jitter theories, and can be extracted efficiently by algorithm from SPICE-level descriptions of any oscillator or VCO. Using *LC* and ring oscillators as test cases, we confirm the ability of nonlinear phase macromodels to capture injection locking, and also obtain significant computational speedups over full SPICE-level circuit simulation. Furthermore, we show that our approach is equally effective for capturing the dynamics of transition to locking, including unlocked tones and phase jump phenomena.

Index Terms—Adler, circuit simulation, differential equations, injection locking, nonlinear macromodels, oscillator phase response.

I. INTRODUCTION

INJECTION locking is an interesting and useful phenomenon universally observed in all kinds of physical oscillators. The term refers to the fact that, under certain conditions, when an oscillator is perturbed by an external weak signal that is close (but not identical) to the oscillator's natural frequency, the oscillator's frequency changes to become identical to that of the perturbing signal, i.e., it "locks" to the external signal. The phenomenon can be observed in many natural systems, from the synchronized blinking of fireflies to electronic systems and lasers, and it is used to advantage in many practical applications. For example, low-cost high-performance quadrature local oscillators that rely on injection locking have been proposed [10]. In optics, injection locking has been used in lasers, for example, to reduce linewidth and frequency noise [14], [13]. Various types of injection-locked oscillators are used as building blocks in phase-locked loops (PLLs) for clock recovery and frequency synchronization.

Despite its widespread use in circuits, the simulation of injection locking presents challenges. Direct simulation of oscillators at the SPICE level is usually inefficient and inaccurate. In practical applications, it can take an oscillator many thousands of cycles to lock to the external signal, as oscillators require small time steps for even moderately accurate simulation. As a result, a method to capture injection locking without performing full circuit simulation is of great interest.

Prior approaches for predicting injection locking have been based on classic simplified treatments such as the Adler equation [1] and Kurokawa's method [11]. Although these approaches provide excellent intuition, as well as basic quantitative metrics for understanding the phenomenon, they rely strongly on approximations such as ignoring nonlinearities and neglecting higher-order harmonics, resulting in inaccurate predictions if the circuit deviates significantly from these assumptions. Moreover, these methods are not completely general, having been derived for *LC* oscillators; indeed, they require the Q factor of the oscillator [1], an inherently *LC*-tank concept. As a result, they cannot be applied to other topologies, such as ring oscillators or multivibrators, for which Q factors cannot easily be defined or calculated.

The study of the behavior of the *unlocked* driven oscillator [17] is also of great interest, as it is important for understanding the operation and bandwidth limitations of injection-locked electronic and laser oscillators. When an external signal does not succeed in putting an oscillator into lock, the oscillator displays periodic variations of frequency and amplitude. Using Adler's theory, Armand [2] developed an analytical approach for finding the output spectra of the unlocked driven oscillator. Armand's method is useful for understanding the unlocked behavior of oscillators; however, it suffers from similar limitations as Adler's, i.e., it can only be applied to oscillators with an explicit Q factor, relies on simplifications, etc.

To circumvent full-circuit simulation during oscillator design, a common methodology is to replace the full oscillator circuit with a much smaller *phase-domain macromodel* [16]. A variety of phase macromodels are available, all based on *linear integration* of a perturbing input to generate output phase deviation (e.g., [3], [8], [9], [12], [19], and [20]). In this paper, we look into the question of qualitative and quantitative accuracy of oscillator phase macromodels for predicting the locked and unlocked behavior of oscillators. We first show that linear phase macromodels for oscillators suffer from a qualitative deficiency: they are incapable of predicting locking behavior. We then propose the use of *nonlinear phase macromodels* as general-purpose replacements for the linear ones that have thus far been used. The nonlinear phase macromodels, related to a recent theory for computing phase noise in oscillators [4], consist

The authors are with the Department of Electrical and Computer Engineering, University of Minnesota, Minneapolis, MN 55455 USA (e-mail: laixl@ece.umn.edu; jr@ece.umn.edu).

of a single scalar nonlinear differential equation for phase devia-
tions. These macromodels can be simulated directly in the time
domain with deterministic injection inputs. A great advantage
of the proposed technique is that nonlinear phase macromodels
can be extracted in an automated fashion from SPICE-level cir-
cuit descriptions or systems of differential equations, using effi-
cient numerical procedures [5]. In contrast to prior approaches,
the proposed technique applies uniformly and generally to any
kind of oscillator, regardless of operating mechanism.

Numerical results demonstrate that the nonlinear phase
macromodel is able to predict locking accurately and efficiently
on *LC* and ring oscillators, with computed phases matching
full oscillator simulations acceptably well. Even for relatively
small oscillator circuits, computational improvements of
almost two orders of magnitude are obtained with the nonlinear
phase-domain macromodel. Such speedups make it possible
to fully investigate the maximum locking range of oscillators
under different injection strengths: the relationship between
injection strength and maximum locking range can be easily
generated and plotted in a few minutes, providing designers
detailed information and intuition about the conditions under
which oscillators lock to external signals. We also verify, with
numerical simulations, our proof that using linear oscillator
macromodels does not succeed in capturing injection locking
at all.

The remainder of this paper is organized as follows. In
Section II, we show that linear phase macromodels are
fundamentally incapable of capturing injection locking. In
Section III, we review the nonlinear phase macromodel and
introduce its use for predicting injection locking and analyzing
the unlocked behavior of oscillators. In Section IV, we present
simulation results on *LC* and ring oscillators.

II. INJECTION LOCKING AND PREVIOUS OSCILLATOR MACROMODELS

Injection locking occurs when an external signal with fre-
quency f is injected into an oscillator whose free-running fre-
quency f_0 is close to f. The oscillator can lock to the injected
signal in both phase and in frequency. We illustrate the con-
cept of injection locking using the simple *LC* oscillator circuit
shown in Fig. 1, where $b(t)$ represents a current injected into the
oscillator.

Fig. 2 depicts the capacitor voltage over two different time pe-
riods. In these two figures, the output voltage of the oscillator is
overlaid with the injected current, scaled in amplitude. Fig. 2(a)
depicts the situation when the current is first injected into the os-
cillator circuit. From the relative shifts of the peaks of the wave-
forms, it can be seen that initially, the oscillator is not locked to
the injected signal. Fig. 2(b) depicts the signal waveforms when
the oscillator has run approximately 500 cycles. Locking is evi-
dent: the oscillator's waveform is perfectly synchronized to that
of the injected signal.

The obvious computational method for analyzing injection
locking is to simulate the oscillator circuit at the SPICE level,
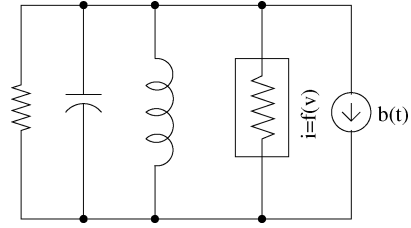and to compare the circuit's response to the injected signal. Un-

Fig. 1.   Simple negative-resistance *LC* oscillator.

fortunately, time-domain simulation of full oscillator circuits is
often inefficient and time consuming since oscillators can re-
quire thousands of cycles to lock, with each cycle requiring
many small time steps. In addition, full circuit simulation can
be inaccurate and inconvenient when the perturbation amplitude
is very small (e.g., 1% of the oscillator's operating amplitude),
as the beat note—periodic variations of frequency and ampli-
tude—due to the perturbation is so small as to be difficult to
observe manually from time-domain waveforms.

To overcome these drawbacks, macromodeling approaches
have been proposed in which the phase of the oscillator's re-
sponse is obtained directly. Two such approaches are reviewed
briefly below.

A. Impulse Sensitivity Function (ISF) Phase Macromodel

In [9], a linear phase macromodel based on a conjecture for
decomposing perturbations into two orthogonal components—a
pure phase deviation and an amplitude deviation—was devel-
oped. The phase shift $\phi(t)$ caused by the injected signal is given
by

$$\phi(t) = \sum_{k=1}^{n} \int_{-\infty}^{\infty} h_\phi^k(t,\tau) i_k(\tau) d\tau. \tag{1}$$

The summation is over all n injected noise current sources i_k in
the circuit, and the impulse response $h_\phi^k(t,\tau)$ to the kth noise
source is given by [9]

$$h_\phi^k(t,\tau) = \frac{\Gamma_k(\omega_0 \tau)}{q_{\max}^k} u(t-\tau) \tag{2}$$

where $q_{\max}^k$ is the maximum charge displacement across the ca-
pacitor on node k, $u(t)$ is the unit step function, and $\Gamma_k(\omega_0\tau)$
is the ISF [9] for the noise source injected at node k. The ISF is
a periodic function with period $2\pi/\omega_0$ that attempts to capture
the phase shift resulting from applying a unit impulse at time
$t = \tau$ at node k.

If all the state variables are nodal voltages of the form

$$V_k(t) = A_k \cdot f_k \left[\omega_0 t + \phi_k + \phi(t)\right] \tag{3}$$

where A_k is the amplitude of the waveform on node k, and f_k
is the normalized waveform of node k, then the ISF $\Gamma_k(x)$ can
be written as

$$\Gamma_k(x) = \frac{f_k'}{\sum_{j=1}^{n} f_j'^2} \tag{4}$$

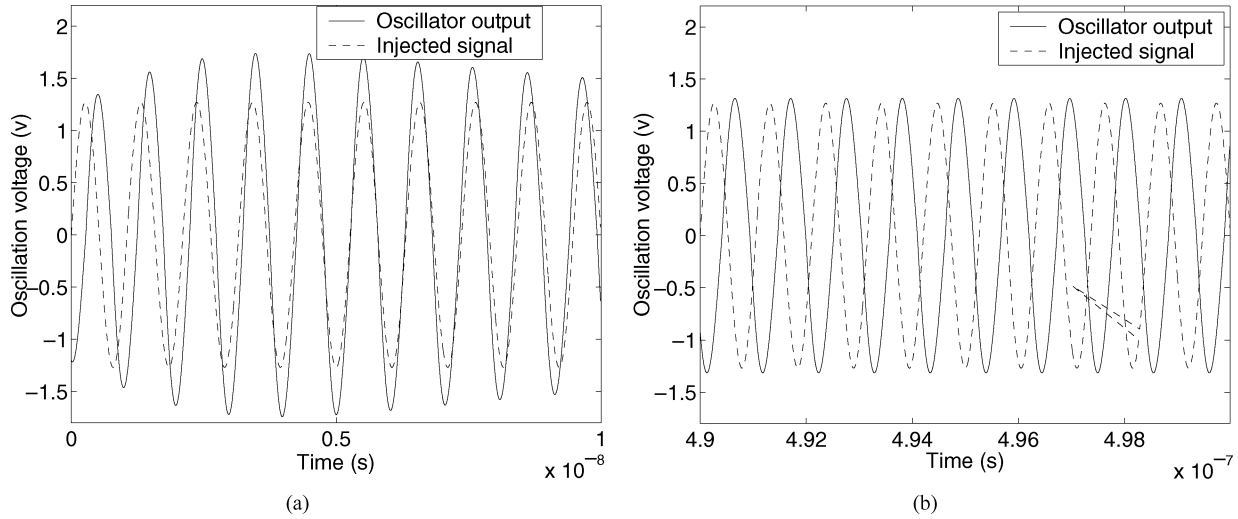where f_k' represents the derivative of the normalized waveform
on node k.

Fig. 2. Injection locking in *LC* oscillator. At the beginning, the oscillator does not lock to the injected signal. After 500 cycles, the oscillator locks to the injected signal with a constant phase difference. (a) Unlocked (initially). (b) Locked (after many cycles).

B. Behavioral Macromodel Based on Perturbation Analysis and Averaging

In another linear macromodeling approach [20], a behavioral phase macromodel based on the idea of perturbation analysis and averaging was presented for harmonic oscillators. We briefly review the essentials of this approach.

A general ordinary differential equation (ODE) form for harmonic oscillator is

$$\frac{d}{dt}i(t) = \frac{v(t)}{L}$$
$$\frac{d}{dt}v(t) = -\frac{i(t)}{C} - \frac{1}{C}I(v(t), \dot{v}(t), t) \qquad (5)$$

where C and L is the effective capacitance and inductance of the resonant tank of the harmonic oscillator, respectively, while $I(v(t), \dot{v}(t), t)$ represents the nonlinear feedback system. Equation (5) can be normalized as

$$\frac{d}{d\bar{t}}\bar{i}(\bar{t}) = \bar{v}(\bar{t})$$
$$\frac{d}{d\bar{t}}\bar{v}(\bar{t}) = -\bar{i}(\bar{t}) - \epsilon f(\bar{v}(\bar{t}), \dot{\bar{v}}(\bar{t})\bar{t}) \qquad (6)$$

with new variables $\bar{t} = \omega_0 t$, $\bar{v}(\bar{t}) = v(\bar{t})/V_0$, $\bar{i}(\bar{t}) = i(\bar{t})/\omega_0 C V_0$, $f(\bar{v}(\bar{t}), \dot{\bar{v}}(\bar{t}), \bar{t}) = I(v(t), \dot{v}(t), t)/I_{\max}$, and $\epsilon = I_{\max}/\omega_0 C V_0$. Here, V_0 is the amplitude of the voltage swinging over the capacitor C, $I_{\max}$ is the maximum current delivered by the feedback system, and ω_0 is the resonant frequency of the *LC* tank. Using vector notation, (6) can be expressed as

$$\frac{dx}{d\bar{t}} = \mathbb{L}x + \epsilon g\left(x, \frac{dx}{d\bar{t}}, \bar{t}\right) \qquad (7)$$

where $x = [\bar{i}(\bar{t}), v(\bar{t})]^T$ and $g = [0, f(\bar{v}(\bar{t}), \dot{\bar{v}}(\bar{t}), \bar{t})]^T$. Hence, the oscillator system can be partitioned into two parts: a resonant tank $dx/d\bar{t} = \mathbb{L}x$ and a feedback sources $\epsilon g(x, dx/d\bar{t}, \bar{t})$. The feedback sources are considered to be perturbations to the resonant tank.

The solution of the resonant tank can be written as $x(\bar{t}) = [A\sin(\bar{t} + \theta), A\cos(\bar{t} + \theta)]^T$. If we introduce a new vector $p = [A, \theta]^T$, then the solution of (7) can be expressed as $x(\bar{t}) = x_s(p, \bar{t})$. If the resonant tank is perturbed, p will change slowly with time. Thus, the solution of (7) can be given by

$$x(\bar{t}) = x_s(p(\bar{t}), \bar{t}). \qquad (8)$$

Using $p(t)$ as the new state variable of the oscillator and substituting (8) into (7), we have

$$\frac{d}{d\bar{t}}p(\bar{t}) = \epsilon h_p(p(\bar{t}), \bar{t}) \qquad (9)$$

where $h_p(p, \bar{t}) = [(\partial x_s/\partial p)(p, \bar{t})]^{-1} g(x_s(p, \bar{t}), (\partial x_s/\partial \bar{t})(p, \bar{t}), \bar{t})$. The averaging method [7] is then applied to eliminate fast-varying processes in (9) and yeild the oscillator macromodel. The macromodel approximates the averaged amplitude and phase obtained from perturbation analysis using a large time step, thus reducing computational cost.

Although aspects of such linear phase macromodels are appealing and useful, one issue they face is that they are unable to capture injection locking. We now prove that any linear model of the form

$$\phi(t) = \int_0^t h(t, \tau) b(\tau) d\tau \qquad (10)$$

where $b(\tau)$ is the injected signal and $h(t, \tau)$ is any periodic phase sensitivity function with the same frequency as that of the free-running oscillator is incapable of capturing injection locking. Note that (8) subsumes simple linear time invariant phase macromodels that are often used to approximate the phase response of oscillators.

Since the oscillator locks to the injected signal $b(t)$, or "catches up" with the phase of the injected signal, we have the relationship

$$\omega_0 t + \phi(t) = \omega_1 t + \theta$$

or

$$\phi(t) = (\omega_1 - \omega_0)t + \theta \qquad (11)$$

where ω_0 is the frequency of the free-running oscillator, ω_1 is the frequency of the injected signal, and θ is a constant, which represents the phase difference between the locked oscillator and injected signal. Equation (11) encapsulates the basic intuition that if the oscillator locks, the phase shift due to the injected signal should grow with time linearly, with a slope of $\omega_1 - \omega_0$. From (10), the phase deviation $\phi(t)$ is the integral of the product of the phase sensitivity function $h(t, \tau)$ and the injected signal $b(\tau)$, which implies $h(t, \tau)b(\tau)$ should have a dc component that equals $\omega_1 - \omega_0$.

Since the phase sensitivity function $h(t, \tau)$ has the same frequency ω_0 as the free-running oscillator, and the frequency of $b(t)$ is very close, but not equal, to ω_0, there are no common frequencies in these two periodic functions. From the orthogonality of trigonometric series, we know that the product of $h(t, \tau)$ and $b(t)$ can, therefore, have no dc component. This contradicts the requirement for injection locking that $h(t, \tau)b(\tau)$ has a dc component that equals $\omega_1 - \omega_0$. Hence, we have shown that no linear phase macromodel, even if time varying, can capture injection locking.

III. NONLINEAR PHASE-DOMAIN MACROMODEL

Here, we provide a brief overview of the nonlinear phase macromodel in [4], which we adapt in this study to predict injection locking and analyze unlocked driven oscillators efficiently. A general ODE for a perturbed oscillator is

$$\dot{x} = f(x) + b(t) \tag{12}$$

where $\dot{x} = f(x)$ is the circuit equation of the unperturbed oscillator [e.g., (21)], $b(t)$ is the perturbation to the free-running oscillator. In developing the nonlinear phase model, the perturbed oscillator solution is shown to be of the form

$$x_s\big(t + \alpha(t)\big) + y(t) \tag{13}$$

where $x_s(t)$ is the unperturbed periodic steady-state response of the oscillator. The effect of the perturbation $b(t)$ to the oscillator results in two phenomena: a *phase shift* $\alpha(t)$ to the unperturbed oscillator and an *orbital deviation* $y(t)$. The phase shift $\alpha(t)$, usually the quantity of greater importance in applications, can be shown [4] to be governed by the following nonlinear differential equation:

$$\dot{\alpha}(t) = v_1^T\big(t + \alpha(t)\big) \cdot b(t). \tag{14}$$

In the above equation, $v_1(t)$ is called the perturbation projection vector (PPV); it is a periodic vector function of time, with the same period as that of the unperturbed oscillator. A key difference between the nonlinear phase model (14) and traditional linear phase models is the inclusion of the phase shift $\alpha(t)$ inside the PPV $v_1(t)$. $\alpha(t)$ in the nonlinear phase model has units of time; the equivalent phase shift, in radians, can be obtained by multiplying $\alpha(t)$ by the free-running oscillation frequency ω_0.
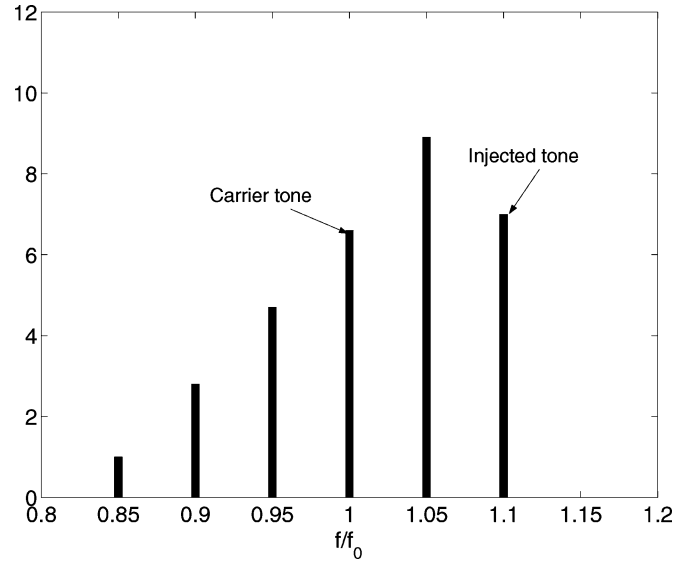

Fig. 3. Typical power spectrum, unlocked driven oscillator.

A. Capturing Injection Locking Using Nonlinear Phase Macromodel

If an oscillator locks to an injected signal, the phase shift $\phi(t)$ must satisfy (11). This phase shift can be calculated by solving the nonlinear phase macromodel (14). Since the phase shift $\alpha(t)$ in (14) has units of time, we can multiply the phase shift $\alpha(t)$ by free-running frequency ω_0 and obtain the phase shift in radians

$$\phi(t) = \omega_0 \alpha(t). \tag{15}$$

Substituting (15) in (11), we have

$$\omega_0 \alpha(t) = (\omega_1 - \omega_0)t + \theta \tag{16}$$

or

$$\alpha(t) = \frac{\Delta\omega_0}{\omega_0}\, t + \frac{\theta}{\omega_0} \tag{17}$$

where $\Delta\omega_0 = \omega_1 - \omega_0$. Thus, the phase shift $\alpha(t)$ should change with time linearly with a slope of $\Delta\omega_0/\omega_0$.

This relationship provides a direct method for predicting locking behavior in oscillators by simulating (14) and checking the slope of the phase deviation $\alpha(t)$ or, equivalently, by plotting $\dot{\alpha}(t)$. For example, if solving (14) for an oscillator injected with a perturbation signal of frequency 10% higher than its free-running frequency results in a phase shift $\alpha(t)$ that increases linearly with a slope of 0.1, we can conclude that the oscillator is locked by the injected signal. Since (14) is a simple one-dimensional nonlinear differential equation that can be solved efficiently by numerical methods, this approach offers large speedups over full simulation since the computational complexity of solving (14) is largely independent of the size of the original circuit. As noted earlier, the PPV of the oscillator can be extracted once from its SPICE-level circuit description via efficient numerical methods, and then used in (14) to investigate injection locking under different frequencies and strengths of the injected signal. In contrast, during full circuit simulation, the whole system of equations for the circuit must be solved.
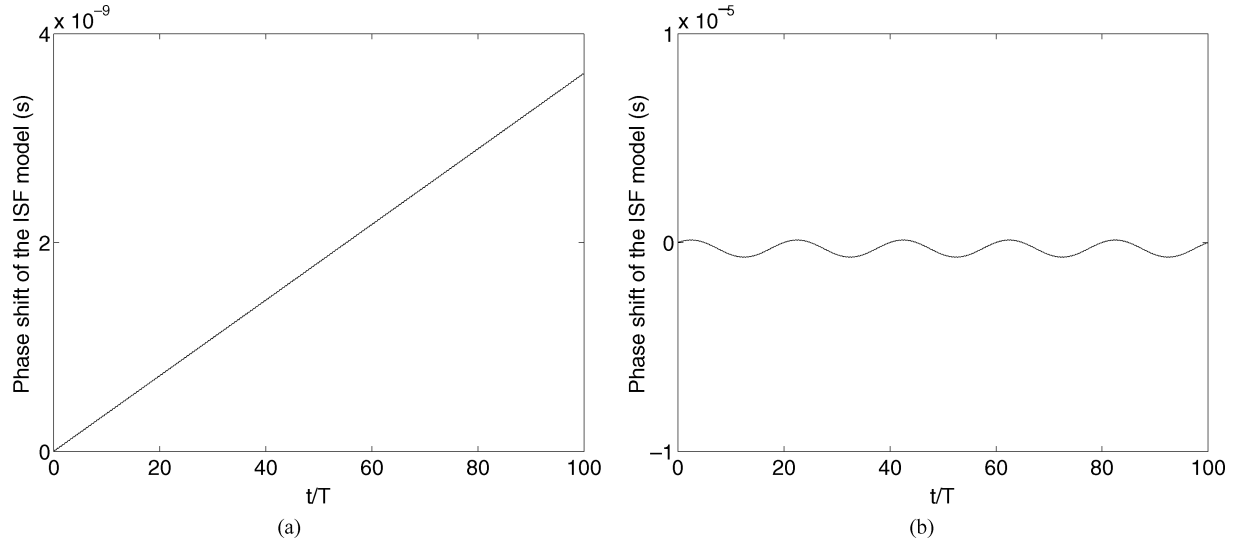
Fig. 4. Phase shift in the *LC* oscillator from the ISF model. (a) Injection current has the same frequency as the *LC* oscillator. (b) Injection current has the frequency 5% lower than the *LC* oscillator.

B. Sideband Prediction in Unlocked Driven Oscillators

When an oscillator is perturbed by an injected signal, but not locked to it, the output spectrum of the *unlocked* driven oscillator is characterized by a nonsymmetric sideband distribution around the carrier. A number of sideband frequency tones are generated around the oscillator's carrier frequency tone, but they all fall on one side of the injected tone, as shown in Fig. 3.

Using Adler's equation, Armand [2] derived analytical expressions for the spectral components of unlocked driven oscillators. The output voltage of the driven oscillator is given by

$$\mathcal{E} = E e^{j\omega_1 t} e^{j\alpha(t)} \tag{18}$$

where E is the voltage amplitude of the free-running oscillator, ω_1 is the frequency of the injected signal, and $\alpha(t)$ is the phase difference between the free oscillator and injected signal. $e^{j\alpha(t)}$ can be expressed in Fourier series form as

$$e^{j\alpha(t)} = j \tan\frac{\theta}{2} + \frac{1 - \tan^2\frac{\theta}{2}}{j\tan\frac{\theta}{2}} \sum_{n=1}^{\infty} \left(j\tan\frac{\theta}{2}\right)^n e^{jn(\Omega t + \theta)} \tag{19}$$

where $\sin\theta = (1/2Q)(E_1/E)(\omega_0/\Delta\omega_0)$ and $\Omega = \Delta\omega_0 \cos\theta$. Multiplying (19) by $E e^{j\omega_1 t}$ provides the spectra of the unlocked driven oscillator.

In addition to predicting injection locking, the nonlinear macromodel (14) can also correctly predict the spectra of the unlocked driven oscillator. The solution of the perturbed oscillator can be expressed as (13). If the amplitude of the injected signal is small, the amplitude deviation $y(t)$ can be ignored and the solution of the driven oscillator can be approximated to be

$$x(t) = x_s\big(t + \alpha(t)\big). \tag{20}$$

Since the phase shift $\alpha(t)$ can be simulated by solving (14) using numerical methods, the time-domain solution of the driven oscillator can be calculated by evaluating (20) with the computed $\alpha(t)$. Performing a Fourier transform on this time-domain solution provides the output spectrum of the unlocked driven oscillator.

The advantage of using the nonlinear macromodel (14) is that, unlike Armand's equation, which applies only to *LC* oscillators, it is valid for any oscillator, while providing large speedups over full SPICE-level simulation. Moreover, using (14) provides more accurate results than Armand's equation, as can be seen in Section IV.

IV. EXPERIMENTAL RESULTS: INJECTION LOCKING AND UNLOCKED SPECTRA

Here, the methods discussed in Sections II and III are applied to analyze the locked and unlocked behavior of two types of oscillators, i.e., *LC* and ring. For both oscillators, we run simulations using full system simulation, the linear phase macromodel, and the nonlinear phase macromodel (14) to study injection locking. For the unlocked driven case, we apply full simulation, the nonlinear macromodel, and the Armand equation to the *LC* oscillator; for the ring oscillator, we use only full simulation and the nonlinear macromodel since Armand's equation is not applicable.

A. 1-GHz LC Oscillator

The differential equations for this *LC* oscillator are

$$\frac{d}{dt}i(t) = \frac{v(t)}{L}$$
$$\frac{d}{dt}v(t) = -\frac{i(t)}{C} - \frac{v(t)}{RC} - \frac{S}{C}\tanh\left(\frac{G_n}{S}v(t)\right) \tag{21}$$

where L, R, and C are the inductance, resistance, and capacitance of the *LCR* tank. S and G_n are parameters of the nonlinear negative resistor that enables oscillations: S determines the amplitude of the oscillation, and G_n is the gain of the nonlinear amplifier. The circuit exhibits autonomous oscillations when $-G_n > 1/R$.

The circuit was simulated with the following parameters: $L = 2.5 \times 10^{-8}/(2\pi)$ H, $C = 4 \times 10^{-11}/(2\pi)$ F, $R = 100~\Omega$,

$S = 1/R$, and $G_n = -10/R$. With these selected parameters, the *LC* tank has a resonant frequency of 1 GHz, and the oscillator has an operating voltage of 1.2 V and an operating current of 52 mA.

1) Full Circuit Simulation: Full system simulation was first carried out to verify locking. The injection current was $b(t) = 0.0052 \sin(\omega t)$, where ω was chosen to be 5% lower than the frequency of the free-running oscillator. The circuit was simulated for approximately 500 cycles to reach the steady state. The simulation results are plotted together with the injected signal, scaled in amplitude. Locking can be clearly seen in Fig. 2(b).

2) ISF Phase Macromodel: The *LC* oscillator is a second-order system. Using the method in [9], the ISF $\Gamma_k(x)$ can be calculated by evaluating (4). Substituting the computed $\Gamma_k(x)$ in (1), we obtain the phase shift $\phi(t)$ under perturbation.

We first applied an injection current with the same frequency as that of the free-running oscillator. For this particular input $b(t) = 0.0052 \sin(\omega_0 t)$, we expect that the phase shift will converge to a constant value since the injected signal has the same frequency as the oscillator. Fig. 4(a) depicts the simulation of phase shift using the ISF model. A constant phase shift is not seen in this figure; on the contrary, the phase of the oscillator increases linearly with time unboundedly. We then applied an injection current with frequency 5% lower than that of the free-running oscillator, the correct phase shift decreases with time linearly, with a slope of 0.05. As expected, the ISF-based result, shown in Fig. 4(b), is incorrect.

These numerical experiments confirm our proof in Section II that the linear phase macromodel cannot capture oscillator injection locking.

3) Behavioral Model Based on Perturbation Analysis and Averaging: We also applied the behavioral model [20] to study injection locking in this *LC* oscillator. The injection current is again assumed to be $b(t) = 0.0052 \sin(\omega_0 t)$, where ω_0 is the free oscillation frequency of the *LC* oscillator. The perturbation $n = [0, \ 0.0052 \sin(\omega_0 t)]^T$ was applied to the right-hand side of (5). Thus, the feedback source $\epsilon h_p(p, \bar{t})$ in (9) can be expressed as

$$\epsilon h_p(p, \bar{t})$$
$$= \frac{J^{-1}}{CV\omega_0} \left[\begin{array}{c} 0 \\ -\dfrac{v(\bar{t})}{R} - S \tanh \left(\dfrac{G_n}{S} v(\bar{t}) \right) + 0.0052 \sin(\bar{t}) \end{array} \right]$$
(22)

where $C = 4 \times 10^{-11}/(2\pi)$ F, $R = 100 \ \Omega$, $V = 1.2$ V, $\omega_0 = 2\pi \times 10^9$, and

$$J = \left[\begin{array}{cc} \sin(\bar{t} + \theta) & A \cos(\bar{t} + \theta) \\ \cos(\bar{t} + \theta) & -A \sin(\bar{t} + \theta) \end{array} \right].$$
(23)

We chose the averaging function as

$$M[h_P](p, \bar{t}) = \frac{1}{T} \int_{\bar{t} - T/2}^{\bar{t} + T/2} h_p(p, \tau) d\tau.$$
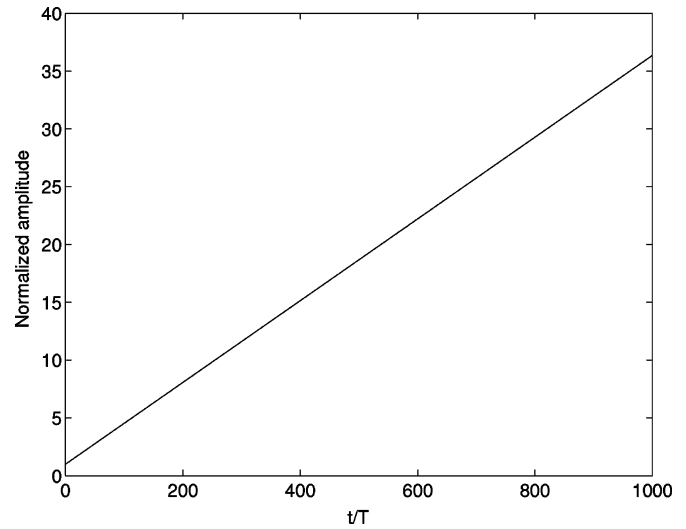(24)

Fig. 5.   Normalized amplitude $A(t)$ of the *LC* oscillator using behavioral model.

By averaging $\epsilon h_p(p, \bar{t})$ for different values of $(A, \theta, \bar{t})$, we developed the oscillator model for this *LC* oscillator. We simulated this oscillator for 1000 cycles using this behavioral model; the normalized amplitude of the oscillator is shown as Fig. 5. From the simulation result, we observe that the amplitude of oscillation $A(t)$ increases with time almost linearly and without an upper bound. This result is incorrect, confirming that this behavioral model is unsuitable for predicting injection locking.

4) Nonlinear Phase Macromodel: Finally, we applied the nonlinear phase (14) to predict injection lock behavior in the *LC* oscillator. We ran simulations for two cases: one in which the injection current has the same frequency as that of the free-running oscillator; the other with a frequency 5% lower. For case 1, we expect the phase shift to converge to a constant, after an initial transient period, while case 2, since the frequency of the injection current differs by 5% from that of the free-running oscillator, $\alpha(t)$ is expected to change linearly with a slope of $\Delta\omega_0/\omega_0 \simeq 0.05$, when the oscillator is in lock.

We observe from Fig. 6(a) that the phase shift does converge to a constant, unlike the linear phase macromodels above. From Fig. 6(b), $\alpha(t)$ indeed decreases linearly with a slope of approximately 0.05, as expected. The simulation results verify that the nonlinear phase macromodel is capable of capturing injection locking correctly.

Using the nonlinear phase macromodel leads to significant speedups in simulation time. In the 1-GHz *LC* oscillator example, the runtime in MATLAB for full circuit transient simulation is 720 s for a simulation time of 400 cycles. However, it takes only 8 s to simulate the same number of cycles using the nonlinear phase macromodel—an approximately 90 times speedup. For the nonlinear phase model, the PPV $v_1(t)$ only needs to be computed once and is reusable for multiple injection locking analyses of the same oscillator.

By solving (14) with different perturbations, the relationship between injection amplitude and maximum locking range of
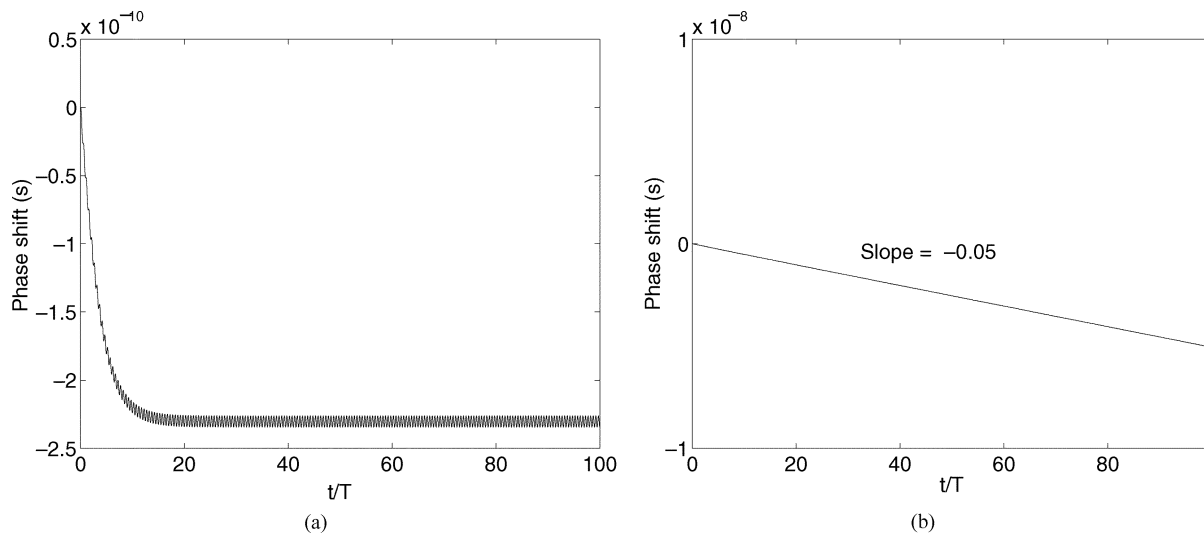
Fig. 6. Phase shift in the *LC* oscillator using the nonlinear phase macromodel. (a) Injection current has the same frequency as the free-running oscillator. (b) Injection current has the frequency 5% lower than the free-running oscillator.
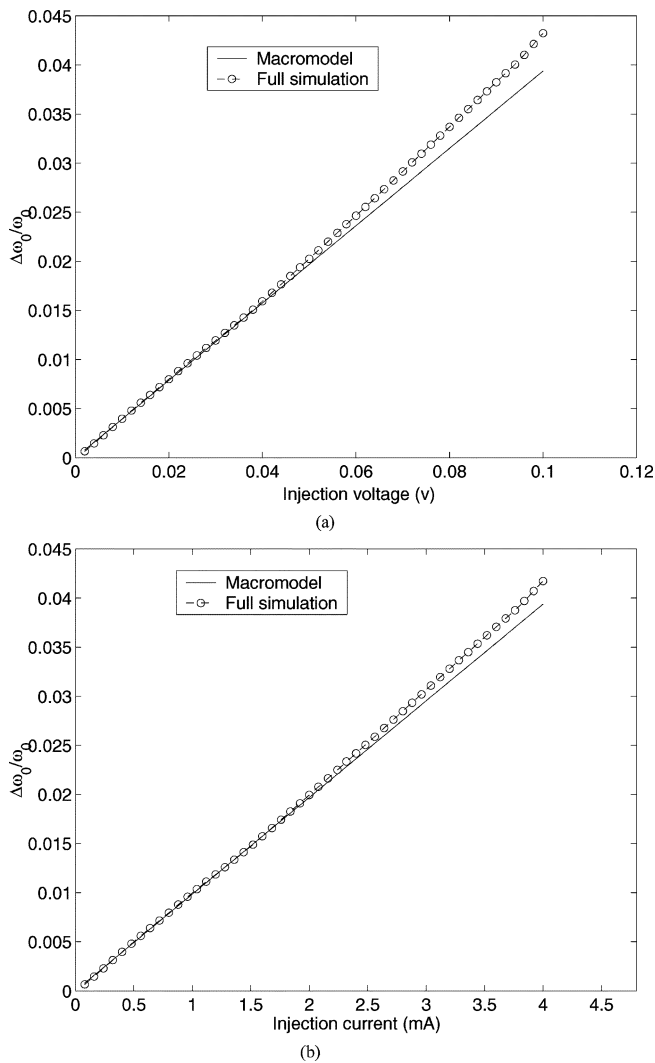

Fig. 7. Relationship between injection amplitude and maximum locking range of the *LC* oscillator. (a) Voltage injection. (b) Current injection.

the oscillator is easily plotted, as shown in Fig. 7. The horizontal axis shows the injection amplitude, while the vertical

axis shows the corresponding maximum locking range, normalized to the oscillator's free-running frequency ω_0. The nonlinear macromodel predicts the maximum locking range well when the injection amplitude is smaller than approximately 10% of the oscillator's operating amplitude. When the injection amplitude becomes larger, the nonlinear macromodel, which is partially based on small-signal perturbation analysis, starts losing accuracy. This is not a significant drawback in most practical applications, where injection amplitudes are typically very small (e.g., 1% of the oscillator's operating amplitude).

On an AMD Athlon 2200+ processor-based workstation running MATLAB on Linux, the nonlinear macromodel plots the figure in 10 min; in contrast, the full simulation (implemented in the same MATLAB environment) needs several hours for a simple high Q LC oscillator when the injection amplitude is small and the injection frequency is close to the oscillator's maximum locking range. The plot provides a quick means to estimate injection locking in the LC oscillator: if a given injected signal falls below the curve, the oscillator locks to the injected signal; otherwise, injection locking does not occur.

5) Phase Jumps and Transients in the Injection-Locked Oscillator: If an oscillator locks to a frequency very close to its maximum locking range, the lock can be unstable: a small perturbation can drive the injection-locked oscillator out of lock, resulting in "jumps" in phase. This phenomenon, noted by many previous researchers [18], [6], [15], is important in determining the stability of injection-locked oscillators. To study phase jumps in the injection-locked oscillator, we inject a current $b(t) = 0.0026 \sin(1.025\omega_0 t)$ to the LC oscillator. From Fig. 7(b), we know that this injection current is very close to the LC oscillator's maximum locking range. When the oscillator is in lock, we apply a small impulse perturbation to this locked oscillator and observe the output.

We simulated this situation using both full simulation and the nonlinear macromodel; the results are shown in Fig. 8. Initially, the oscillator locks to the injected signal and the phase shift grows linearly, as shown in Fig. 8(b). At time $t = 100T$, we
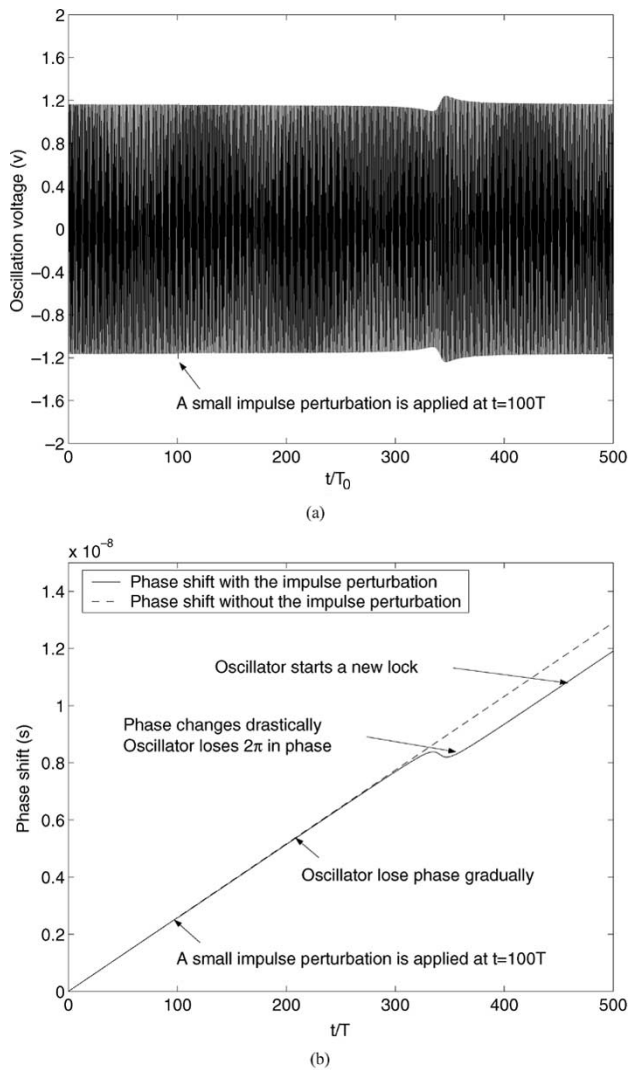
Fig. 8. Simulation of phase jump in the injection-locked oscillator. (a) Full simulation. (b) Nonlinear phase macromodel.

apply a small impulse current to the locked oscillator. We can observe from Fig. 8(b) that the phase shift of the oscillator starts to slow down. At time $t = 340T$, the phase of the oscillator changes drastically. Finally, the oscillator loses 2π in phase and starts a new lock after $t = 400T$. The waveform of the full simulation shown in Fig. 8(a) displays a strong frequency and amplitude deviation at $t = 340T$, which matches the drastic phase change predicted by simulating the nonlinear phase macromodel.

6) Output Spectra of the Unlocked Driven Oscillator: A perturbation current $b(t) = 0.0026 \sin(1.03\omega_0 t)$ is now injected into the *LC* oscillator. Fig. 7(b) shows that the *LC* oscillator will not lock under this perturbation. The output spectrum for this case is calculated using full SPICE-level simulation, the nonlinear phase macromodel and the Armand equation; the results are compared in Fig. 9. It can be seen that the nonlinear phase macromodel matches full simulation very well. The run time of the full SPICE-level simulation implemented in MATLAB is approximately 1 h for a simulation length
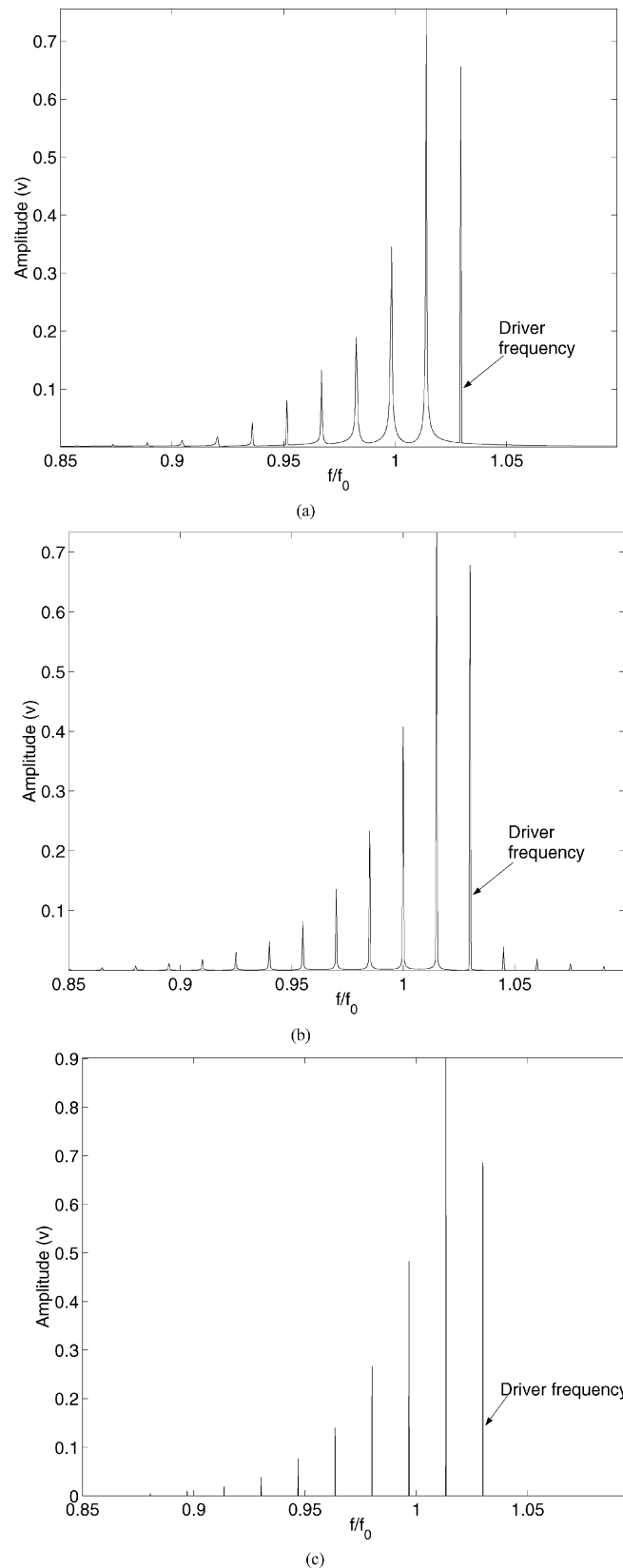

Fig. 9. Output spectra of the unlocked driven *LC* oscillator. (a) Full simulation. (b) Nonlinear macromodel. (c) Armand's equation.

of 2000 cycles; in contrast, the nonlinear phase macromodel takes only 40 s to simulate the same number of cycles—about a 90 times speedup, without significant loss of simulation
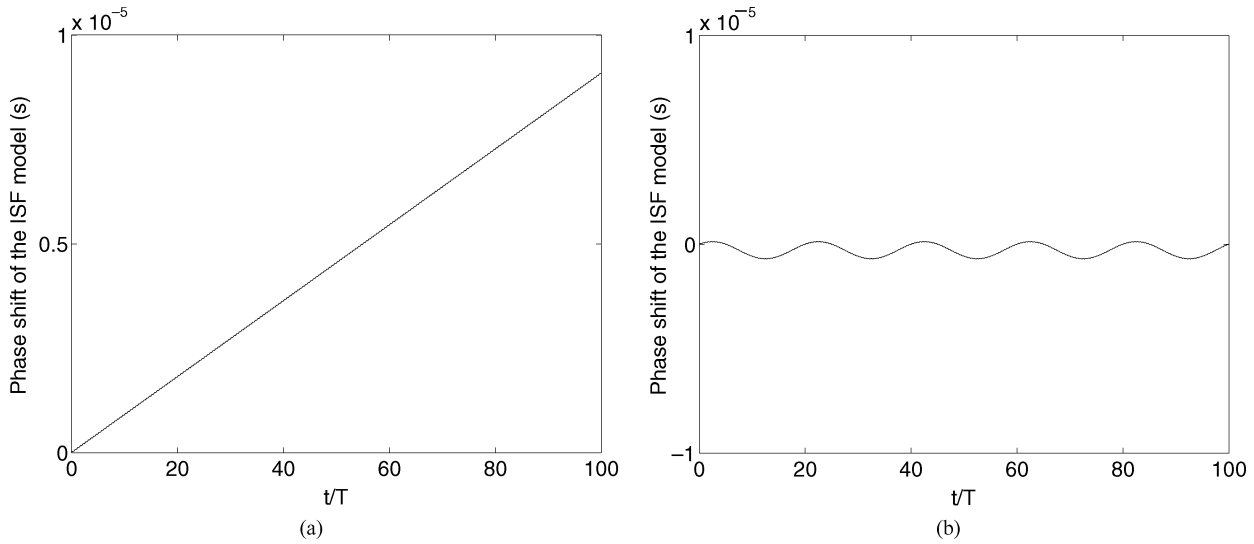
Fig. 10. Phase shift in the ring oscillator using the ISF model. (a) Injected signal has the same frequency as the ring oscillator. (b) Injected signal has frequency 5% lower than the ring oscillator.
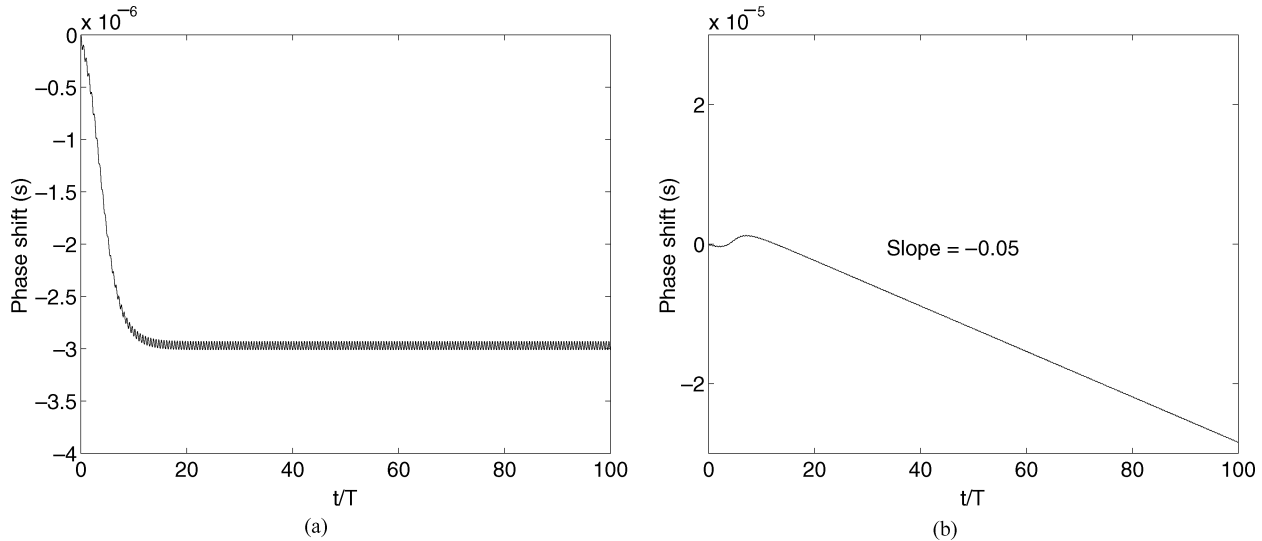

Fig. 11. Phase shift in the ring oscillator using the nonlinear phase macromodel. (a) Injection current has the same frequency as the ring oscillator. (b) Injection current has frequency 5% lower than the ring oscillator.

accuracy. The Armand equation, being an analytical equation, is, of course, the fastest method to produce the output spectra of the driven oscillator; however, its accuracy is not as good as the nonlinear phase macromodel's, as can be seen in Fig. 9.

B. 153-kHz Three-Stage Ring Oscillator

The three-stage ring oscillator is described by the following differential equations:

$$\dot{v}_1(t) = -\frac{v_1}{R_1 C_1} + \frac{\tanh\left(G_{m3} v_3(t)\right)}{R_1 C_1} \tag{25}$$

$$\dot{v}_2(t) = -\frac{v_2}{R_2 C_2} + \frac{\tanh\left(G_{m1} v_1(t)\right)}{R_2 C_2} \tag{26}$$

$$\dot{v}_3(t) = -\frac{v_3}{R_3 C_3} + \frac{\tanh\left(G_{m2} v_2(t)\right)}{R_3 C_3}. \tag{27}$$

Assuming identical stages, we set $C_1 = C_2 = C_3 = 2$ nF, $R_1 = R_2 = R_3 = 1$ kΩ, and $G_{m1} = G_{m2} = G_{m3} = -5$. The peak current drawn by each stage of the oscillator from the power supply is 1.2 mA.

Simulation results for the ring oscillator using the linear ISF model, with injection currents of the same frequency as, and frequency 5% lower than, the free-running oscillator, are shown in Fig. 10. Again, the ISF model is unable to capture phase-locking behavior. The behavioral model [20] is not applicable to this ring oscillator since the behavioral oscillator model is developed for, and only applicable to, harmonic oscillators.

In Fig. 11(a) and (b), phase shifts in the ring oscillator due to injection currents with the same frequency as, and frequency 5% lower than, the free-running oscillation frequency are shown. As with the LC oscillator, the nonlinear model accurately predicts phase locking caused by the injected current.
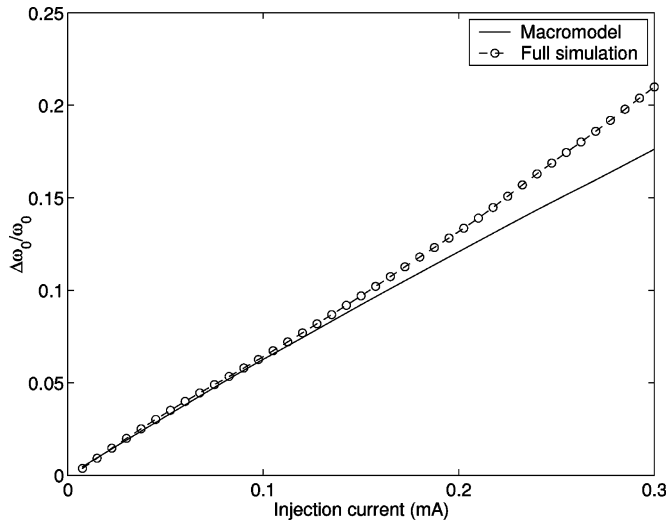
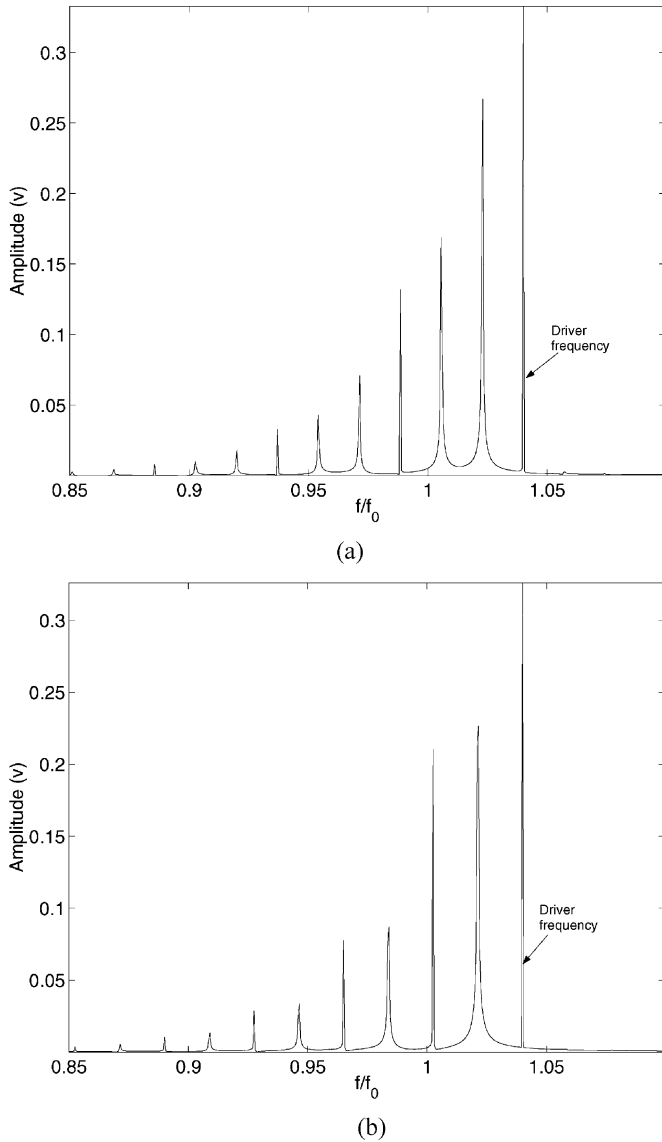Fig. 12. Relationship between injection amplitude and maximum locking range of the ring oscillator.

Fig. 13. Output spectra of the unlocked driven ring oscillator. (a) Full simulation. (b) Nonlinear macromodel.

Similar to the *LC* oscillator case, we plot the relationship between injection amplitude and maximum locking range of the ring oscillator in Fig. 12. The nonlinear macromodel predicts injection locking well when the amplitude of injection current is below 0.2 mA–approximately 15% of the ring oscillator's peak current. Analytical methods derived from *LC* oscillator principles, such as Adler's equation, cannot be applied to the ring oscillator, as the operating mechanisms are very different. To find the output spectra of the unlocked driven ring oscillator, we inject a perturbation current $b(t) = 0.00006 \sin(1.03\omega_0 t)$. Fig. 13 shows a good match between full simulation and the nonlinear macromodel. As before, Armand's analytical equation cannot be applied in this case since it requires the Q factor, which is not easily defined for ring oscillators.

V. CONCLUSIONS

We have proposed and demonstrated the use of algorithmically extracted nonlinear phase-domain macromodels of oscillators for prediction injection-locking related phenomena. Prior methods based on linear integration have been shown to be qualitatively inadequate for this purpose. We have demonstrated that the nonlinear macromodels correctly predict not only injection locking, but also unlocked spectra, phase jumps, and transients. Simulations using the nonlinear phase macromodel provide significant speedups compared to SPICE-level simulation, even for relatively small circuits. Further use of (13) appears promising for capturing amplitude-related phenomena in oscillators as well.

REFERENCES

[1] R. Adler, "A study of locking phenomena in oscillators," in *Proc. IRE Waves and Electrons*, vol. 34, June 1946, pp. 351–357.
[2] M. Armand, "On the output spectrum of unlocked driven oscillators," *Proc. IEEE*, vol. 57, pp. 798–799, May 1969.
[3] A. Demir, E. Liu, A. L. Sangiovanni-Vincentelli, and I. Vassiliou, "Behavioral simulation techniques for phase/delay-locked systems," in *Proc. Custom Integrated Circuits Conf.*, May 1994, pp. 453–456.
[4] A. Demir, A. Mehrotra, and J. Roychowdhury, "Phase noise in oscillators: A unifying theory and numerical methods for characterization," *IEEE Trans. Circuits Syst. I*, vol. 47, pp. 655–674, May 2000.
[5] A. Demir and J. Roychowdhury, "A reliable and efficient procedure for oscillator PPV computation, with phase noise macromodeling applications," *IEEE Trans. Computer-Aided Design*, vol. 22, pp. 188–197, Feb. 2003.

[6] M. C. Espana-Boquera and A. Puerta-Notario, "Noise effects in injection locked laser simulation: Phase jumps and associated spectral components," *Electron. Lett.*, vol. 32, no. 9, pp. 818–819, Apr. 1996.

[7] M. I. Freidlin and A. D. Wentzell, *Random Perturbations of Dynamical Systems*. New York: Springer-Verlag, 1998.

[8] M. Gardner, *Phase-Lock Techniques*. New York: Wiley, 1966.

[9] A. Hajimiri and T. H. Lee, "A general theory of phase noise in electrical oscillators," *IEEE J. Solid-State Circuits*, vol. 33, pp. 179–194, Feb. 1998.

[10] P. Kinget, R. Melville, D. Long, and V. Gopinathan, "An injection-locking scheme for precision quadrature generation," *IEEE J. Solid-State Circuits*, vol. 37, pp. 845–851, July 2002.

[11] K. Kurokawa, "Injection locking of microwave solid state oscillators," *Proc. IEEE*, vol. 61, pp. 1386–1410, Oct. 1973.

[12] J. Lee, K. S. Kundert, and B. Razavi, "Modeling of jitter in bang–bang clock and data recovery circuits," in *Proc. Custom Integrated Circuits Conf.*, Sept. 2003, pp. 711–714.

[13] H. Li and K. N. B. Abraham, "Analysis of the noise spectra of a laser diode with optical feedback from a high-finesse resonator," *IEEE J. Quantum Electron.*, vol. 25, pp. 1782–1793, Aug. 1989.

[14] T. Ohta and K. Murakami, "Reducing negative resistance oscillator noise by self-injection," *Electron. Commun. Jpn.*, vol. 51-B, pp. 80–82, Oct. 1968.

[15] A. E. Siegman, *Lasers*. Herndon, VA: Univ. Sci. Books, 1986.

[16] J. L. Stensby, *Phase-Locked Loops: Theory and Applications*. New York: CRC, 1997.

[17] H. L. Stover, "Theoretical explanation for the output spectra of unlocked driven oscillators," *Proc. IEEE*, vol. 54, pp. 310–311, Feb. 1966.

[18] M. R. Surette, D. R. Hjelme, R. Ellingsen, and A. R. Mickelson, "Effects of noise on transients of injection locked semiconductor lasers," *IEEE J. Quantum Electron.*, vol. 29, pp. 1046–1063, Apr. 1993.

[19] M. Takahashi, K. Ogawa, and K. S. Kundert, "VCO jitter simulation and its comparison with measurement," in *Proc. Design Automation Conf.*, June 1999, pp. 85–88.

[20] P. Vanassche, G. G. E. Gielen, and W. Sansen, "Behavioral modeling of coupled harmonic oscillators," *IEEE Trans. Computer-Aided Design*, vol. 22, pp. 1017–1026, Aug. 2003.

Xiaolue Lai received the B.S. and M.S. degrees in automatic control from the University of Science and Technology of China, Hefei, China, in 1993 and 1996, respectively, the M.S. degree in electrical engineering from the University of Minnesota, Minneapolis, in 2001, and is currently working toward the Ph.D. degree in electrical engineering at the University of Minnesota.

From 2001 to 2002, he was a Logic Design Engineer with Sandcraft Inc., Santa Clara, CA. His research interests include macromodeling, and fast simulation and noise analysis of mixed-signal circuits, especially oscillators and PLLs.

Jaijeet Roychowdhury received the Bachelor's degree in electrical engineering from the Indian Institute of Technology, Kanpur, India, in 1987, and the Ph.D. degree in electrical engineering and computer science from the University of California at Berkeley, in 1993.

From 1993 to 1995, he was with the Computer-Aided Design (CAD) Laboratory, AT&T Bell Laboratories, Allentown, PA. From 1995 to 2000, he was with the Communication Sciences Research Division, Bell Laboratories, Murray Hill, NJ. From 2000 to 2001, he was with CeLight Inc. (an optical networking startup), Silver Spring, MD. Since 2001, he has been with the Electrical and Computer Engineering Department and the Digital Technology Center, University of Minnesota, Minneapolis. His professional interests include the design, analysis, and simulation of electronic, electrooptical, and mixed-domain systems, particularly for high-speed and high-frequency communications. He holds ten patents.

Dr. Roychowdhury was named an IEEE Circuits and Systems (IEEE CAS) Society Distinguished Lecturer for 2003–2004. He was cited for Extraordinary Achievement by Bell Laboratories in 1996.